Fano-like resonance characteristics of asymmetric Fe_2O_3@Au core/shell nanorice dimer*

Wang Bin-Bing(王彬兵), Zhou Jun(周 骏)†, Zhang Hao-Peng(张昊鹏), and Chen Jin-Ping(陈金平)

Institute of Photonics, Faculty of Science, Ningbo University, Ningbo 315211, *China*

(Received 29 November 2013; revised manuscript received 16 February 2014; published online 10 June 2014)

A geometrical configuration of Fe_2O_3/Au core-shell nanorice dimer is proposed and its multipolar plasmon Fano-like resonance characteristics are theoretically investigated by generalizing the plasmon hybridization model of individual nanorice to the bright and dark modes of the nanorice dimer. Under the irradiation of polarization light, the extinction spectra of the nanorice dimer are numerically simulated by using the finite element method (FEM). Our studies show that the Fano-like resonance of the nanorice dimer results in an asymmetric line shape of the Fano dip in the extinction spectrum which can be controlled by varying the structure parameters of the nanorice dimer. Meanwhile, there is a giant field enhancement at the gap between the two nanorices on account of the plasmonic coupling in the nanorice dimer. The aforementioned two characteristics of the nanorice dimer are useful for plasmon-induced transparency and localized surface plasmon resonance sensors.

Keywords: localized surface plasmon resonance, field enhancement, nanorice, plasmon hybridization

PACS: 73.22.Lp, 81.07.–b, 73.20.Mf **DOI:** 10.1088/1674-1056/23/8/087303

1. Introduction

The noble metallic nanostructures have attracted extensive attention because their electronic and optical properties are significant in various applications such as nonlinear optics,[1] molecular specific imaging and spectroscopy,[2,3] surface-enhanced Raman scattering (SERS),[4] and biological sensing.[5] As is well known, the optical absorption, scattering, and near-field electromagnetic intensities of noble metallic nanostructures are strongly affected by their LSPR properties which depend sensitively on the nanoparticle size, morphology, metal type, and the permittivity of the surrounding medium, making it possible to excogitate the electric and magnetic responses in a wide scope.[6–8] Especially, for a metallic nanostructure with greater geometrical complexity, the coherent interference between a super-radiant bright mode and a subradiant dark mode of the nanostructure can form the antibonding and the bonding plasmon modes and is used to describe the optical response behaviors of the complex metal nanostructures.[9,10] Moreover, it is interesting that the coherent interference between the bright and dark modes may make a distinct Fano dip in the extinction spectrum of a metallic nanostructure.[11,12] Zhang *et al*.[13] have found that Fano resonances are actually expressed as the superposition of the narrow dark multipolar mode of nanoring and the broad bright dipolar mode of nanodisk, as a result, to give rise to deep tunable Fano dips in the scattering spectra of the disk-ring plasmonic nanostructure. Zhou *et al*.[14] have further reported that Fano resonance produced by the plasmon coupling between Au nanorod array and semicontinuous gold nanoparticle film has a much stronger local field enhancement than a continuous thin film, leading to over two orders of magnitude enhancement in the photoluminescence. Numerous studies also demonstrate that compared with the case of elementary plasmon modes of the nanoparticle, the plasmonic Fano interference is very sensitive to the surrounding dielectric medium due to the distinctive microscopic mechanism of Fano resonance,[12] and the sharp and asymmetric response line shape of Fano resonance is beneficial to increasing the figure of merit of plasmonic sensors.[15] Therefore, Fano resonance can enormously enhance the sensitivity for plasmonic sensing. Besides, Fano resonance in photoinduced doping of graphene can enhance the photocurrent to obtain prominent carrier density.[16,17] Besides, the prominent carrier density in photo-induced doping graphene can be obtained by Fano resonance.[16,17]

Over the past several decades, considerable research efforts have been devoted to the excogitation, fabrication, and synthesis of various plasmonic nanostructures, such as nanorods,[18] nanoshells,[19,20] nanorings,[21] nanocubes,[22,23] nanowires,[24,25] and nanocrescents.[26] Among the plenty of contrivable nanostructures, dielectric/metal core–shell composite nanoparticles are of outstanding advantages in the respect of highly structurally tunable plasmon resonances.[27] It is important to determine the internal dielectric material and the external metal as well as the appropriate sizes of the core and shell for achieving optimal

*Project supported by the National Natural Science Foundation of China (Grant Nos. 61275153 and 61320106014), the Natural Science Foundation of Zhejiang Province, China (Grant No. LY12A04002), the International Collaboration Program of the Natural Science Foundation of Ningbo (Grant Nos. 2010D10018 and 2012A610107), K. C. Wong Education Foundation and the K. C. Wong Magna Foundation of Ningbo University, China.

†Corresponding author. E-mail: zhoujun@nbu.edu.cn

© 2014 Chinese Physical Society and IOP Publishing Ltd

plasmon characteristics. In fact, many physical and chemical nanopreparation methods are experimentally proposed to fabricate preciously the metal core–shell nanoparticles. Particularly, by using the wet chemical technique, a new nanostructure composed of a spindle shaped hematite core and a continuous nanometer-thick gold shell, known as nanorice, was first prepared by Wang *et al.*[28] and exhibits some dramatic nanoscale optical properties of both nanorod and nanoshell, such as the intense local fields and the extreme tunable plasmon resonances. Theoretically, Jain and El-Sayed[29,30] have extended Mie theory to demonstrate that the spheroidal silica core-gold nanoshell has a great tunability of the LSPR by changing the shell thickness-to-core radius ratio or the dielectric constant of the surrounding medium. They also found that the LSPR frequency of the spheroidal nanoshell has a remarkable shift due to the increased coupling strength between the inner and outer surface plasmon as the thickness of the gold shell decreases.[31] Khoury *et al.*[32] have further investigated the spatial and spectral responses of the plasmonic fields in the gap of spherical nanoshell dimer. It is discovered that there are stronger enhanced electric field in the gap region between the two nanoparticles and a red shift of the LSPR wavelength when two nanoparticles become closer to each other, which, as a naturally considering result, motivates us to investigate the optical properties induced by Fano resonances of the nanorice dimer with a spindle shaped nanoshell.

In this paper, the optical properties of an Fe_2O_3/Au core–shell nanorice dimer are theoretically investigated by the finite element method (FEM). The physical insight into the optical phenomena is gained by generalizing the plasmon hybridization model of individual nanorice to the bright and dark modes of the nanorice dimer. It is presented that the response line shape of the multipolar plasmon Fano-like resonances can be controlled by modulating the relative positions of the two nanorices in the nanorice dimer. We further show that the coherent coupling of the bright and dark modes can lead to a distinct Fano dip in the extinction spectrum of the nanorice dimer, and that Fano-like resonances evoke giant electric field enhancement at the interparticle gap.

2. Schematic diagram and simulation method

The nanostructure of the nanorice dimer comprised of two identical nanorices is schematically shown in Fig. 1. The nanorice is made up of a dielectric spindle core and an outer Au shell. In our dimer model, the refractive index of inner core of nanorice is 2.94 for hematite, the permittivity data of gold shell are obtained from the bulk experimental result of Johnson and Christy,[33] and the dimer is assumed to be in a vacuum environment. In addition, throughout the paper, the thickness of Au shell, the length and width of the nanorice are fixed at $t = 5$ nm, $h = 150$ nm, and $s = 30$ nm, respectively. A series of numerical simulations is carried out in the incorporated RF module of the commercial software package COMSOL Multiphysics, which contains electromagnetic scattering formula code based on FEM. As a more suitable research method of the near-field optics, FEM is usually used to analyze the optical properties of metallic nanostructures, that is, the electromagnetic problems of complex nanostructures can be effectively handled by solving Maxwell's equations on an appropriate discretized spatial grid.[34,35] In our research, the extinction cross section of the dimer is derived as the sum of the scattering and absorption cross section. The scattering spectra of dimer are calculated by integrating the normalized $\boldsymbol{E}$ field around a far-field transform boundary enclosing the dimer, while the absorption spectra are calculated by integrating time-average resistive heating on the nanorices.[36] The nanorice dimer is illuminated by the incident light with polarization vector parallel to the axis of dimer and propagation direction perpendicular to the axis of dimer. The perfectly matched layers of absorbing boundaries are used to avoid the nonphysical reflections of emergent electromagnetic waves from the grid boundaries.

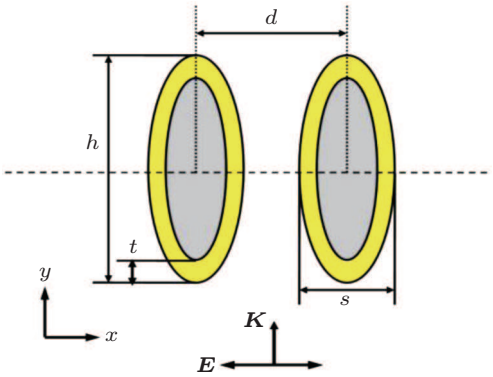


Fig. 1. (color online) Schematic diagram of section plane of the nanorice dimer. t, h,s, d, represent, respectively, the thickness of nanoshell, the outer dimensions along the major axis and the minor axis of nanorice, and the distance between the centers of two nanorices. The axis of the dimer (along the x axis) is set to be the line of centers of two nanorices. $\boldsymbol{E}$ and $\boldsymbol{K}$ are the electric field vector and the wave vector, respectively.

3. Results and discussion

To understand the plasmon resonance coupling mechanism of the proposed dimer, the extinction spectra of individual nanorice are investigated for different values of rotation angle θ and shown in Fig. 2. The polarization of incident light is fixed in a given direction which is along the minor axis of nanorice at $\theta = 0°$. For the sake of clarity, a part of extinction spectra ranging from 600 nm to 850 nm are shown in Fig. 2(b). It can be seen from Figs. 2(a) and 2(b) that when the polarization of incident light is parallel to the minor axis of the nanorice ($\theta = 0°$), the transverse mode dipolar peak and the quadrupole peak occur at 792 nm and 719 nm, respectively, which suggests that only the weak transverse surface plasmons are excited. For the light polarized in the direction perpendicular to the minor axis ($\theta = 90°$), a strong

longitudinal mode dipolar peak appears at 976 nm and a weak quadrupole peak arises at 654 nm. However, for other θ values, the four plasmon resonance peaks H_1, H_2, L_2, and L_1 arise in their extinction spectra and correspond to the principal high-energy peak, the secondary high-energy peak, the secondary low-energy peak, and the principal low-energy peak, respectively, which suggests that both the transverse surface plasmons and the longitudinal surface plasmons are excited. Besides, with the increase of the θ value, the dipole peak experiences a tiny spectroscopic red shift, and the peak value increases rapidly as shown in Fig. 2(a). Whereas, with θ increasing (except 0° and 90°), the intensity of secondary low-energy peak weakens gradually and finally disappears in the extinction spectra.

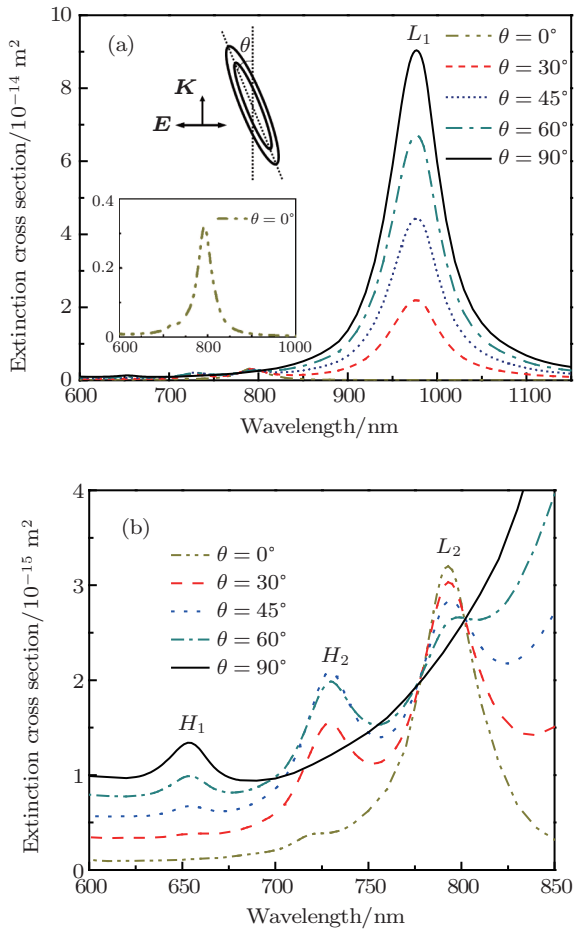


Fig. 2. (color online) (a) Optical extinction spectra of the individual nanorice at various θ values. The upper inset shows the model scheme of the rotated nanorice, θ is the angle between the major axis of nanorice and the wave vector, and the bottom inset shows the magnified spectrum for $\theta = 0°$. (b) The enlarge extinction spectra in a short wavelength range.

The plasmon hybridization theory can explain the physical origin of the plasmon resonance peaks in the extinction spectra of nanorice. For a single nanorice, it can be modeled as a hybrid between a solid prolate spheroid and an ellipsoidal cavity inside a continuous metal. In this case, as shown in Fig. 3, there are four elementary plasmon modes under the incident illumination, i.e., the dipolar mode ($l = 1$) and the quadrupolar mode ($l = 2$) of the prolate spheroid and the dipolar mode ($l = 1$) and the quadrupolar mode ($l = 2$) of the cavity. When $\theta = 0°$, the dipole mode ($l = 1$) is along the minor axis of the ellipsoid or cavity. When $\theta = 90°$, the dipole mode ($l = 1$) is along the major axis of the ellipsoid or cavity. However, for $0° < \theta < 90°$, the dipole mode ($l = 1$) stems from the coupling of two dipole modes which are respectively along the major and minor axis of the ellipsoid or cavity. When θ is equal to 0° or 90° (Fig. 3(a)), only the dipolar–dipolar ($l = 1$) and quadrupolar–quadrupolar ($l = 2$) hybridizations exist in the nanorice since the modes of different angular momenta are forbidden from interacting. The coherent hybridizations of these elementary plasmon modes generate the two high-energy antibonding plasmon modes and the two low-energy bonding plasmon modes. The antibonding modes are not shown in our extinction spectra by reason of their exorbitant energy. The principal low-energy and the secondary low-energy bonding plasmon modes are corresponding to dipole and quadrupole resonance peaks, respectively, in the extinction spectra. However, the selection rule of plasmon hybridization is relaxed in the case of single rotated nanorice (Fig. 3(b)), allowing modes of different angular momenta to interact each other. Therefore, the dipole mode ($l = 1$) of the prolate spheroid can

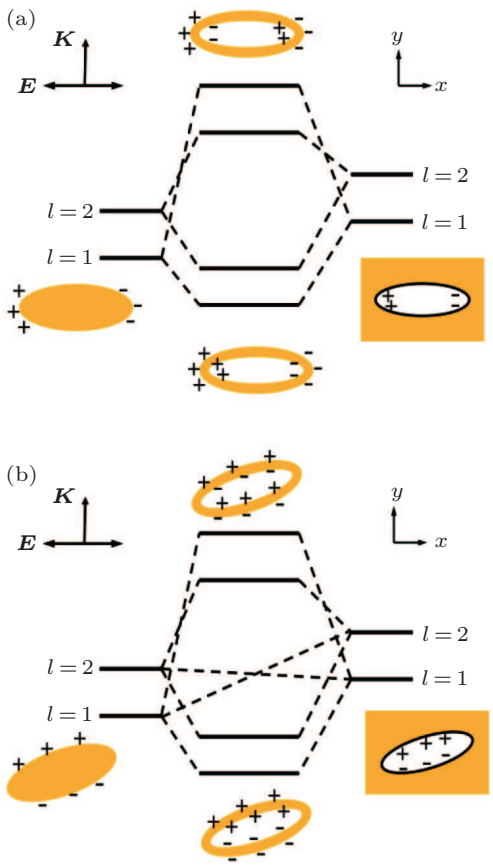


Fig. 3. (color online) For the light polarized in the direction parallel to the x axis, the plasmon hybridization models of the individual nanorice with θ values of (a) 90° and (b) any angle (except 0° and 90°). The image charge distribution of the prolate spheroid and the cavity corresponds to the case of the excited nanorice model.

interact with not only the dipole mode ($l = 1$) of the cavity but also the quadrupole mode ($l = 2$) of the cavity.[37–39] Similarly, the mutual effect resulting from the quadrupole mode ($l = 2$) of the prolate spheroid and the dipole mode ($l = 1$) of the cavity is engendered when the incident light polarization is neither perpendicular nor parallel to the major axis of nanorice. As a consequence, the plasmon hybridization impels to come into being four bonding modes, which are exhibited in the extinction spectra.

Figure 4 shows the extinction spectra of the nanorice dimer with varying θ value for a fixed distance $d = 92$ nm between the two nanorices. The inset in Fig. 4(a) presents the geometry configuration of the nanorice dimer which consists of the static nanorice and the rotated nanorice. Compared with Fig. 2, in Fig. 4(a), the extinction spectrum of dimer at $\theta = 60°$ shows a special line shape which possesses a dip, a principal low-energy peak and a secondary low-energy peak in a wavelength range of 900 nm–1100 nm. The principal and the secondary low-energy peaks, derived from the interaction of the bright and dark modes, are corresponding to bonding mode and antibonding mode respectively.[40] As far as we know, the quadrupolar dark plasmon mode of a long nanorod cannot be excited by the normal incident plane wave, but can be stimulated by a dipole source of the short nanorod in the gold nanorod dimer.[11] Similarly, the dark mode of the static nanorice can be excited by the longitudinal component (along the y axis) of the dipolar bright mode of the rotated nanorice. What is more, the dark mode is coupled with the dipolar bright mode of the rotated nanorice by means of the near field interaction, which will give rise to an asymmetric Fano dip in the extinction spectrum of the dimer.[12,41] In Fig. 4(a), the principal low-energy peaks are located at 993, 997, 1004, 1010, and 1014 nm for $\theta = 15°$, $30°$, $45°$, $60°$, and $75°$ respectively. It is clear that the principal low-energy peaks show a distinct red shift with the increase of angle value but the intensity is enhanced gradually. When $\theta = 0°$, only the transverse plasmon resonances of two nanorices are excited, and the two peaks are found at 725 nm and 794 nm respectively. As angle θ increases to 15°, there is a relatively weak principal low-energy peak in the extinction spectra, that is, the weak superradiant bright mode of the rotated nanorice is produced. Due to the unremarkable dipolar bright mode of the rotated nanorice, the induced dark mode in the other nanorice is so puny and uneasy to be coupled such that the Fano dip cannot be discovered in the extinction spectra. By increasing the rotation angle from 15° to 60°, the bright and the dark plasmon modes are enhanced gradually, and then are coupled to generate a Fano dip which is widened and deepened gradually as shown in Fig. 4(a). When $\theta = 75°$, the Fano dip is absent and there is only a low-energy peak in the extinction spectrum. In this case, the longitudinal component of the dipolar plasmon mode of rotated nanorice is reduced to a tiny value and the corresponding dark mode turns weak. It implies that the strength of the plasmon interaction between the bright and dark modes is faint, and results in a negligible Fano-like resonance, even though the super-radiant bright mode is greatly enhanced.

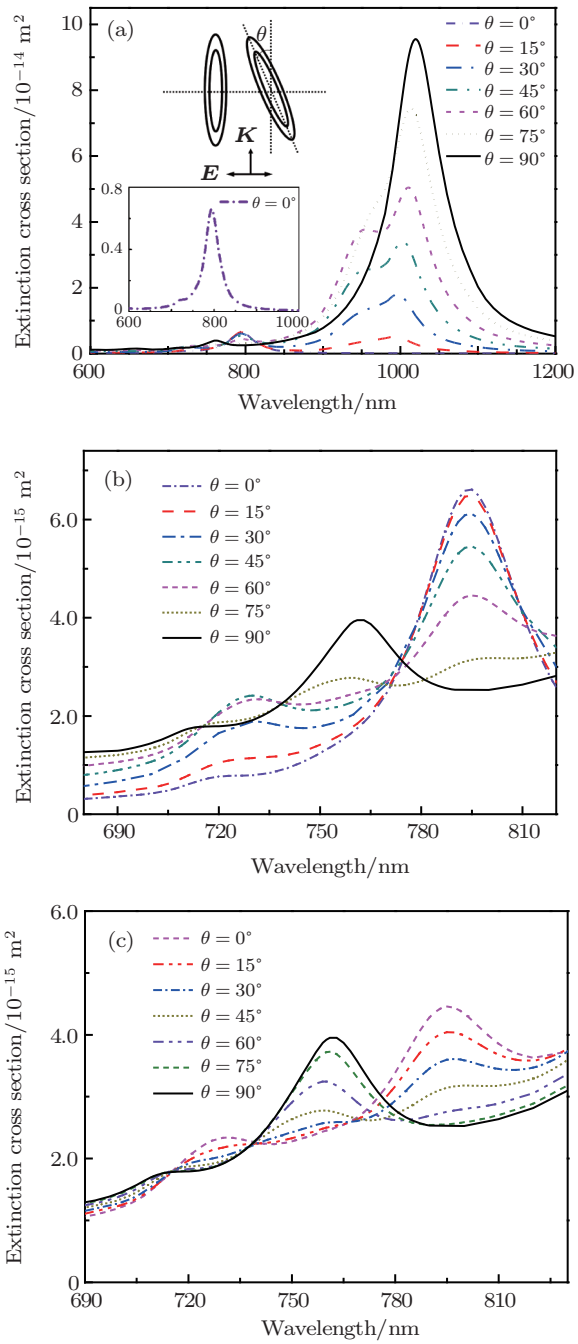


Fig. 4. (color online) (a) Optical extinction spectra of the nanorice dimer at various θ values. The upper inset shows the model scheme of the nanorice dimer, θ is the angle between the major axis of nanorice and the wave vector, the bottom inset shows the magnified spectrum for $\theta = 0°$. (b) The enlarge extinction spectra in a short wavelength range. (c) The details of extinction spectra in a range of rotation angle from 60 ° to 90°.

In addition, for the case of $\theta = 90°$, as shown in Figs. 4(a) and 4(b), the plasmon peaks in the extinction spectrum are located at 713, 762, and 1020 nm respectively. The peak at

713 nm corresponds to the quadrupole mode of the nanorice dimer and the peak at 1020 nm is a result of the dipole plasmon resonance. However, there is no plasmon resonance peak in the region of adjacent 762 nm for θ from 0° to 60° (Fig. 4(b)). So, we further investigate the extinction spectra of the dimer with the rotation angle range of 60°–90°. As shown in Fig. 4(c), with the increase of θ, the plasmon resonance peak around the 762 nm arises and displays a distinct red shift because the dipole bright mode of the rotated nanorice can acquire greater interaction with the inner surface plasmon mode of gold shell of the other nanorice during a tip of the rotated nanorice to be closer to the other nanorice.

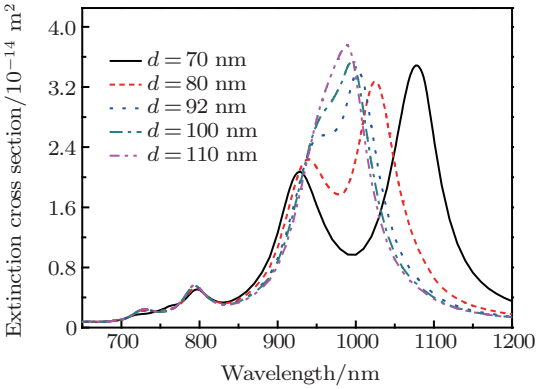


Fig. 5. (color online) Optical extinction spectra of the nanorice dimer for $\theta = 45°$ with different distances between the two nanorices.

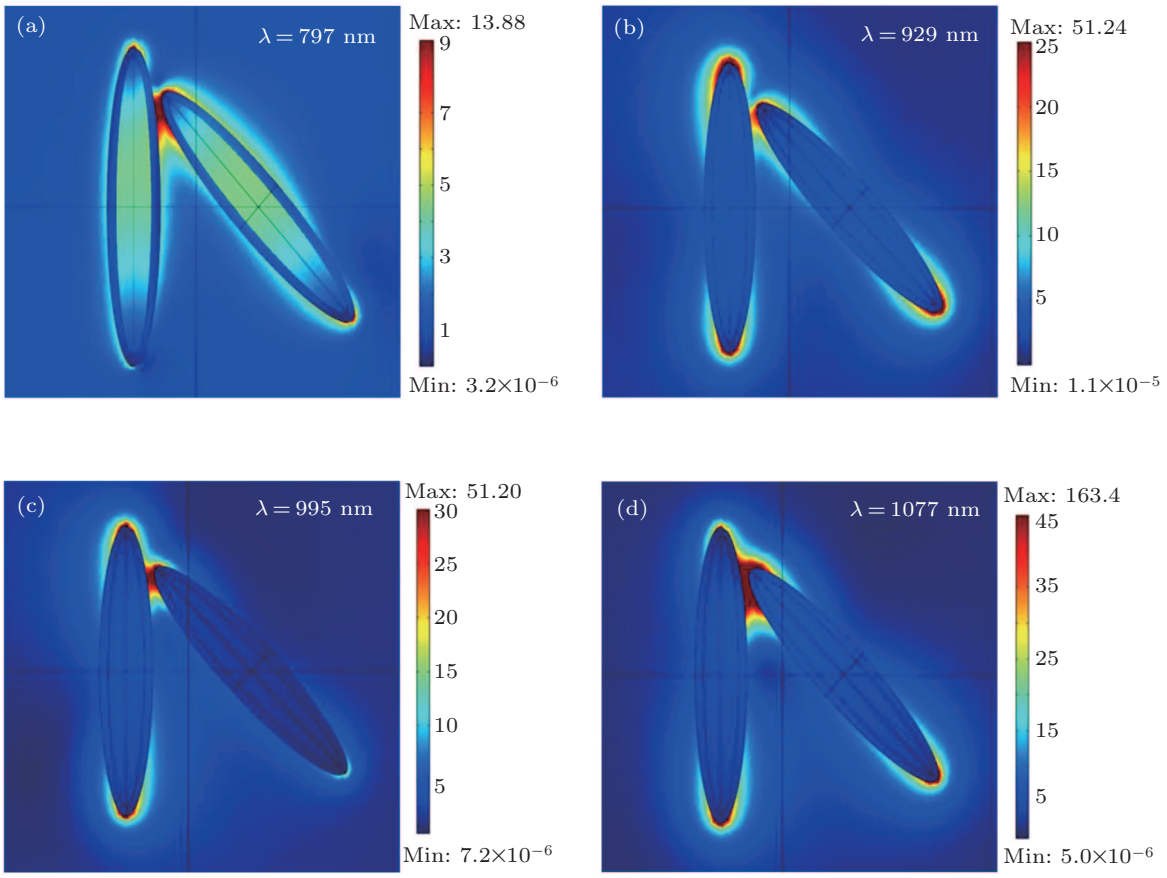


Fig. 6. (color online) Enhancement distributions of electric field amplitudes of the nanorice dimer at $\theta = 45°$ and $d = 70$ nm for the plasmon resonance wavelengths of (a) 797 nm, (b) 929 nm, (c) 995 nm, and (d) 1077 nm.

Furthermore, to comprehend the influence of distance d on the Fano-like resonance, the extinction spectra of the nanorice dimer with varying separation of the two nanorices for a fixed rotated angle 45° are shown in Fig. 5. It is obvious from Fig. 5 that there are a principal high-energy peak at 730 nm, a secondary high-energy peak at 793 nm, and a low-energy peak at 989 nm but no Fano dip in the extinction spectrum for $d = 110$ nm. When $d = 80$ nm, the four plasmon resonance peaks, which are corresponding respectively to the principal high-energy peak (733 nm), the secondary high-energy peak (795 nm), the secondary low-energy peak (938 nm), and the principal low-energy peak (1024 nm), arise in the extinction spectrum, and a distinct Fano dip appears. It indicates that Fano profile occurs only when the distance between the two nanorices is well suited to achieve a relatively strong interaction between the bright and dark modes. And with reducing the distance between the two nanorices, a significant asymmetric Fano dip can be obtained, and the principal and secondary high-energy peaks have a blue shift and a red shift respectively. It is clearly observed that one peak appears at

761 nm denoted as the solid line in the extinction spectrum, yet no peak is found at the nearby wavelength for other distance values. The result shows that the coupling between the plasmon modes of inner and outer surfaces will be supported if the gap between the two nanorices is small enough. In addition, with the d value varying from 100 nm to 70 nm, the principal and secondary low-energy peaks present their great red shifts and blue shifts in the extinction spectra of the nanorice dimer respectively. These results can be explained by the coupling interaction resulting from hybridization theory. The increasing of the interaction between the bright and dark modes could give rise to a larger energy gap between the antibonding and bonding modes, making the antibonding mode peak blue-shifted and the bonding mode peak red-shifted. As shown in Fig. 5, the line width and depth of the Fano dip are also affected by the strength of plasmon coupling interaction. It is presented that the Fano dip becomes progressively wider and deeper with reducing the interparticle separation.

As an example, the enhancement distributions of electric field amplitudes of the nanorice dimer are shown in Fig. 6 for the different plasmon resonance wavelengths. Figure 6(a) exhibits the internal and external surface plasmons in two nanorices excited by the resonance peak at 797 nm corresponding to the tertiary high-energy mode of the dimer. There are distinct enhancements of the electric fields occurring around the tips of two nanorices as shown in Figs. 6(b)–6(d), which arises from the plasmon resonance peaks at 929 nm and 1077 nm corresponding to the antibonding and the bonding modes respectively, and the plasmon resonance peak at 995 nm corresponding to the Fano minimum. It indicates that lower energy plasmon mode will evoke a greater electric field enhancement for the nanorice dimer, and it can also be clearly seen that the main contribution of the electric field enhancement concentrates in the gap and tip region.[38] Comparing Figs. 6(b)–6(d), the enhancement of electric field amplitudes affected by the Fano-like resonance mode is higher than by the antibonding mode but lower than by the bonding mode, and more concentrated in the gap area of the nanorice dimer. Therefore, it is found that all these strong enhanced fields play a role of the plasmon resonance coupling in the nanorice dimer.

4. Conclusions

In this paper, the plasmon resonance characteristics of the individual nanorice and the nanorice dimer are systematically studied by using the three-dimensional FEM method. It is found that two distinct low-energy peaks and a Fano dip in the extinction spectrum of the nanorice dimer are a result of Fano-like resonance, which is caused by the interaction between a dipole bright mode of the rotated nanorice and a dark mode of the other nanorice. With the increasing of the rotation angle, the Fano dip becomes first deep and then shallow in the extinction spectrum of the nanorice dimer. With the decreasing of the interparticle separation, the Fano dip turns deeper and wider and the Fano minimum shows a clear red shift. By adjusting the rotation angle θ of the one nanorice properly and reducing the interparticle separation as much as possible, the distinct Fano dip can be obtained. In addition, the phenomenon of the giant enhancement of local electric fields at the gap of the two nanorices is explained as the result of Fano-like resonance excitation. The results outlined in this paper open up possibilities for using the Fano-like resonances of the nanorice dimer to design the plasmon-induced transparency photonic devices and the chemical and biological sensors.

References

[1] Romani E C, Vitoreti D, Gouvêa P M P, Caldas P G, Prioli R, Paciornik S, Fokine M, Braga A M B, Gomes A S L and Carvalho I C S 2012 *Opt. Express* **20** 5429

[2] Leduc C, Si S, Gautier J, Soto-Ribeiro M, Wehrle-Haller B, Gautreau A, Giannone G, Cognet L and Lounis B 2013 *Nano Lett.* **13** 1489

[3] Stender A S, Marchuk K, Liu C, Sander S, Meyer M W, Smith E A, Neupane B, Wang G F, Li J J and Cheng J X 2013 *Chem. Rev.* **113** 2469

[4] Zhang R, Zhang Y, Dong Z C, Jiang S, Zhang C, Chen L G, Zhang L, Liao Y, Aizpurua J and Luo Y 2013 *Nature* **498** 82

[5] Ruemmele J A, Hall W P, Ruvuna L K and Van Duyne R P 2013 *Anal. Chem.* **85** 4560

[6] Rahmani M, Lei D Y, Giannini V, Lukiyanchuk B, Ranjbar M, Liew T Y, Hong M and Maier S A 2012 *Nano Lett.* **12** 2101

[7] Angelomé P C, Heidari Mezerji H, Goris B, Pastoriza-Santos I, Pérez-Juste J, Bals S and Liz-Marzán L M 2012 *Chem. Mater.* **24** 1393

[8] Ringe E, Zhang J, Langille M R, Sohn K, Cobley C, Au L, Xia Y N, Mirkin C A, Huang J X, Marks L D and Van Duyne R P 2010 *Mater. Res. Soc. Symp. Proc.* **1208** O10

[9] Prodan E, Radloff C, Halas N J and Nordlander P 2003 *Science* **302** 419

[10] Li J N, Liu T Z, Zheng H R, Gao F, Dong J, Zhang Z L and Zhang Z Y 2013 *Opt. Express* **21** 17176

[11] Yang Z J, Zhang Z S, Zhang L H, Li Q Q, Hao Z H and Wang Q Q 2011 *Opt. Lett.* **36** 1542

[12] Miroshnichenko A E, Flach S and Kivshar Y S 2010 *Rev. Mod. Phys.* **82** 2257

[13] Zhang Y, Jia T Q, Zhang H M and Xu Z Z 2012 *Opt. Lett.* **37** 4919

[14] Zhou Z K, Peng X N, Yang Z J, Zhang Z S, Li M, Su X R, Zhang Q, Shan X Y, Wang Q Q and Zhang Z Y 2011 *Nano Lett.* **11** 49

[15] Zhang S, Bao K, Halas N J, Xu H and Nordlander P 2011 *Nano Lett.* **11** 1657

[16] Fang Z Y, Liu Z, Wang Y M, Ajayan P M, Nordlander P and Halas N J 2012 *Nano Lett.* **12** 3038

[17] Fang Z Y, Wang Y M, Liu Z, Schlather A, Ajayan P M, Koppens F H L, Nordlander P and Halas N J 2012 *ACS Nano* **6** 10222

[18] Huang X H, El-Sayed I H, Qian W and El-Sayed M A 2006 *J. Am. Chem. Soc.* **128** 2115

[19] Carpin L B, Bickford L R, Agollah G, Yu T K, Schiff R, Li Y and Drezek R A 2011 *Breast Cancer Res. Treat.* **125** 27

[20] Jiang S M, Wu D J, Cheng Y and Liu X J 2012 *Chin. Phys. B* **21** 127806

[21] Cai Y, Li Y, Nordlander P and Cremer P S 2012 *Nano Lett.* **12** 4881

[22] McLellan J M, Li Z Y, Siekkinen A R and Xia Y N 2007 *Nano Lett.* **7** 1013

[23] Zhou F, Liu Y and Li Z Y 2011 *Chin. Phys. B* **20** 037303

[24] Wu D J, Jiang S M and Liu X J 2012 *Chin. Phys. B* **21** 077803

[25] Deng C Y, Zhang G L, Zou B, Shi H L, Liang Y J, Li Y C, Fu J X and Wang W Z 2013 *Chin. Phys. B* **22** 106102
[26] Fernandez-Dominguez A I, Luo Y, Wiener A, Pendry J B and Maier S A 2012 *Nano Lett.* **12** 5946
[27] Zhang J T, Tang Y, Lee K and Ouyang M 2010 *Science* **327** 1634
[28] Wang H, Brandl D W, Le F, Nordlander P and Halas N J 2006 *Nano Lett.* **6** 827
[29] Jain P K and El-Sayed M A 2007 *Nano Lett.* **7** 2854
[30] Jain P K and El-Sayed M A 2007 *J. Phys. Chem. C* **111** 17451
[31] Hooshmand N, Jain P K and El-Sayed M A 2011 *J. Phys. Chem. C* **2** 374
[32] Khoury C G, Norton S J and Vo-Dinh T 2009 *ACS Nano* **3** 2776
[33] Johnson P B and Christy R W 1972 *Phys. Rev. B* **6** 4370
[34] Brown L V, Sobhani H, Britt Lassiter J, Nordlander P and Halas N J 2010 *ACS Nano* **4** 819
[35] Butet J, Duboisset J, Bachelier G, Russier-Antoine I, Benichou E, Jonin C and Brevet P F 2010 *Nano Lett.* **10** 1717
[36] Knight M W and Halas N J 2008 *New J. Phys.* **10** 105006
[37] Hu Y, Noelck S and Drezek R 2010 *ACS Nano* **4** 1521
[38] Ye J, Lagae L, Maes G, Borghs G and Dorpe P V 2009 *Opt. Express* **17** 23765
[39] Zou W B, Zhou J, Jin L and Zhang H P 2012 *Acta Phys. Sin.* **61** 097805 (in Chinese)
[40] Wu D J, Jiang S M and Liu X J 2012 *J. Phys. Chem. C* **116** 13745
[41] An W, Zhu T and Zhu Q Z 2014 *J. Quantum Spectrosc. Radiat. Transf.* **132** 28